Chinese Journal of Chemical Engineering 70 (2024) 269–279

Contents lists available at ScienceDirect

Chinese Journal of Chemical Engineering

journal homepage: www.elsevier.com/locate/CJChE

Full Length Article

Study on thermal decomposition kinetics of azobenzene-4,4′-dicarboxylic acid by using compensation parameter method and nonlinear fitting evaluation

Shuyi Shen [1], Song Guo [1,*], Sining Chen [2,*], Jinhua Zhao [1]

[1] Nanjing University of Science & Technology, Nanjing 210094, China
[2] China Academy of Safety Science and Technology, Beijing 100012, China

ARTICLE INFO

Article history:
Received 24 November 2023
Received in revised form
8 March 2024
Accepted 14 March 2024
Available online 17 April 2024

Keywords:
Azobenzene-4,4′-dicarboxylic acid
Thermal decomposition behavior
Kinetic mechanism
Thermal hazard evaluation
Compensation parameter effect

ABSTRACT

Recently, azobenzene-4,4′-dicarboxylic acid (ADCA) has been produced gradually for use as an organic synthesis or pharmaceutical intermediate due to its eminent performance. With large quantities put into application in the future, the thermal stability of this substance during storage, transportation, and use will become quite important. Thus, in this work, the thermal decomposition behavior, thermal decomposition kinetics, and thermal hazard of ADCA were investigated. Experiments were conducted by using a SENSYS evo DSC device. A combination of differential iso-conversion method, compensation parameter method, and nonlinear fitting evaluation were also used to analyze thermal kinetics and mechanism of ADCA decomposition. The results show that when conversion rate α increases, the activation energies of ADCA's first and main decomposition peaks fall. The amount of heat released during decomposition varies between 182.46 and 231.16 $J \cdot g^{-1}$. The proposed kinetic equation is based on the Avrami–Erofeev model, which is consistent with the decomposition progress. Applying the Frank-Kamenetskii model, a calculated self-accelerating decomposition temperature of 287.0 °C is obtained.

1. Introduction

Azo-compounds (azos) are widely and traditionally used in textile, food, cosmetics, printing, and other industries. They are particularly useful as initiators of polymerization in chemical production [1]. As an example, azobenzene can undergo photo-isomerization and form response under the stimulation of ultraviolet and visible-light irradiation, heat, and other stimuli. It has been used to produce a thin film of photo-responsive superlattice that is directly manipulated by light [2]. This feature is also concerned by the biomedical community, where azobenzene is used in high-resolution, real-time, low-toxicity biological imaging, in the preparation of light-conversion drugs to enhance their controllability in terms of time and position, and in the achievement of controlled drug release in tumor treatment [3]. Similarly, azobenzene-4,4′-dicarboxylic acid (ADCA) can be used to produce metal-organic frameworks (MOFs) with porous structures, providing possibilities for diverse scenarios such as gas storage, separation, ion exchange, drug delivery, and so on [4]. Additionally, photo-responsive MOFs also perform well in dye adsorption of Congo red in contaminated water [5]. Due to its excellent performance, ADCA, an azobenzene derivative, is currently progressively rising in popularity as an intermediate used to create organic materials, photosensitive materials, and other materials.

However, researchers did not pay much attention to the thermal decomposition mechanism of azos, such as ADCA, and the risk characteristics associated with combustion and explosion events resulting from thermal decomposition. When heated, the structure's N=N double bond (as seen in Fig. 1) is easy to break and can release about −100–−180 $kJ \cdot mol^{-1}$ standard decomposition enthalpy [6]. On July 22, 2011, 300 kg of 2,2′-azobis (2,4-dimethyl) valeronitrile (ABVN, which has a structure similar to ADCA) was illegally transported by a large sleeper bus on the section of the expressway connecting Beijing and Zhuhai in Henan Province, China. The 300 kg of ABVN was heated and decomposed due to a combination of friction, engine heat release, and other factors, which led to a deflagration accident. As a result, 41 people died, and

* Corresponding authors. Tel.: +8613951836507.
E-mail addresses: guosong@njust.edu.cn (S. Guo), chensn@chinasafety.ac.cn (S. Chen).

https://doi.org/10.1016/j.cjche.2024.03.015
1004-9541/

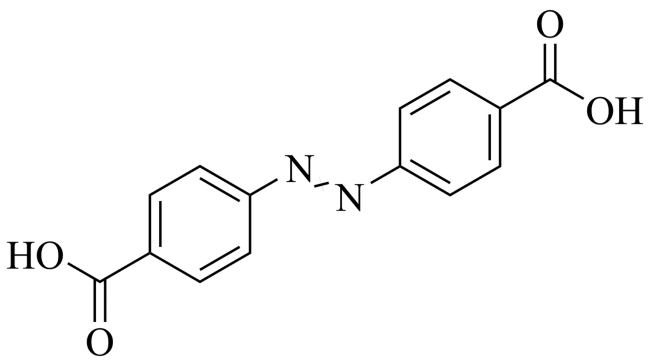

Fig. 1. The structure formula of ADCA.

six got injured. Besides, the direct economic loss was up to CNY 23.4206 million [7]. In the future, when azobenzene derivatives are applied on a large scale, their thermal stability over the course of their whole life cycle will inevitably become the focus of attention.

Till now, scholars at home and abroad have carried out a series of works on thermal safety of azos. On the one hand, scholars paid attention to the acquisition of kinetic and thermodynamic properties of these materials. Liu *et al.* [8] studied the thermal decomposition behavior of 2,2′-azobis-2-methylbutyronitrile, 2,2′-azobisisobutyramidine hydrochloride (AIBA), and 2,2′-azobis *iso*-butyronitrile (AIBN) both in the absence and presence of acid or alkali catalysis. Differential scanning calorimetry (DSC) and thermomechanical analysis III (TAM III) were used during this process. The activation energy was calculated by three different methods, namely Flynn Wall Ozawa method, American society for testing and materials (ASTM) E698 method, and Frank-Kameneskii approximate method. Liu *et al.* [9] measured the apparent exothermic onset temperature, decomposition heat, and apparent exothermic peak temperature of AIBN and ABVN based on DSC. The apparent activation energy and pre-exponential factor in the decomposition process were obtained through Flynn–Wall–Ozawa equation and approximate solution, which is a non-isothermal method. Li *et al.* [10] studied the thermal decomposition process of AIBN under various circumstances through DSC, C80, Dewar bottle, and other experiments. They paid special attention to the initial stage of the reaction, analyzed and concluded that the reaction process at this stage was affected by sublimation or physical phase transition, and endothermic and exothermic effects were in competition with one another. Yu *et al.* [11] also used DSC to investigate the effect of impurities on thermal decomposition behavior of 1-((cyano-1-methylethyl) azo) formamide (CABN). Additionally, they obtained thermodynamic parameters such as heat of decomposition from adiabatic experiments conducted by Phi-TEC II. Apart from DSC, another common method is quality-related analysis, including thermogravimetry (TG) and derivative thermogravimetry (DTG). Çanakçı [12] investigated thermal behaviors of newly synthesized azo monomers and polymers by this method plus differential thermal analysis (DTA). During the research, Coats–Redfern, Horowitz–Metzger, and Broido methods have also been used to determine activation energy, enthalpy, entropy, and Gibbs free energy change at different stages.

On the other hand, scholars concentrated on evaluating thermal risk, using the self-accelerating decomposition temperature (SADT) as the primary indicator. Roduit *et al.* [13] calculated the SADT of AIBN based on the kinetic-based method and heat balance of system and compared it with the experimental results, proving the usefulness of the kinetic-based method. Li *et al.* [14] simulated the SADT of AIBA in a 25-kg box and a 50-kg drum by means of kinetics. Zhou *et al.* [15] used the Semenov thermal spontaneous combustion theory to compute the SADT of 2,2′-azobis (2-methylpropionate) in contact with three incompatible substances.

In addition, some scholars have also explored the micro mechanism of thermal decomposition. Sun *et al.* [16] analyzed the decomposition mechanism and determined the kinetic parameters of azobenzene using the molecular dynamics modeling approach and kinetic calculation method based on the experimental data of SENSYS Evolution DSC. Jia *et al.* [17] conducted experiments on diisopropyl azodicarboxylate (DIAD) by using a C80 microcalorimeter and the STA-FTIR-MS system. The thermal decomposition behavior and decomposition mechanism of DIAD were characterized and analyzed. Tian *et al.* [18] studied the thermal decomposition of CABN and figured out the gaseous products and decomposition residues by using a thermogravimetry-mass spectrometer and an infrared spectrometer. They also obtained optimal thermal decomposition reaction path of CABN by using Gaussian software. Kim *et al.* [19] analyzed thermal decomposition mechanism of water-soluble azo dyes based on their ultraviolet-visible absorbance at various heating temperatures. They suggested that these dyes rapidly decompose within a narrow temperature range following a melting process.

Although previous scholars have carried out a series of studies on azos, the majority of these research studies concentrated on aliphatic azos and gave little thought to the thermal decomposition of azos containing benzene rings. Therefore, in order to determine the kinetic model of the thermal decomposition reaction and deduce the thermal decomposition mechanism of ADCA, this study will first observe the thermal decomposition behavior of ADCA and then calculate the thermodynamic and kinetic parameters of its thermal decomposition reaction. Furthermore, the study will assess the thermal stability of ADCA based on Frank-Kamenetskii (F-K) theory.

2. Experimental

2.1. Instrument and testing conditions

The SENSYS evo DSC device was used in this experiment. There are thermocouple stacks outside the cylindrical measuring area of this instrument, which can measure 94% of the heat exchange between the sample and the reference crucible. When it comes to the working principle, similar to DSC with planar sensing structure, the temperatures of the sample and the reference material are equal under the program control, and the relationship between thermal power difference transmitted to them per unit time and temperature is measured. The measuring temperature range of the calorimeter is room temperature ~830 °C, temperature precision is ±0.02 °C, calorimetric precision is ±0.1%, and the programmable temperature-scanning rate is 0.01–30 °C·min^{-1}. The heating rate selected for this experiment is 1.0, 2.0, 4.0, and 8.0 °C·min^{-1}, which is heated from ambient temperature to 600 °C. The sample information is listed in Table 1.

2.2. Calculation method

In this study, in order to obtain the kinetic parameters of ADCA decomposition reaction, Friedman method was used to determine E_{α_i} and $A_{\alpha_i} f_{\text{real}}(\alpha_i)$ corresponding to different conversion rates α_i, without being affected by the mechanism function. Then the compensation coefficients were determined based on the common solid-state reaction model and compensation effect method [20,21]. Finally, the accuracy of those models was evaluated by nonlinear fitting results. The calculation procedures adopted in this paper are as follows:

Table 1
Sample information

Name	CAS	Manufacturer	State	Purity	Amount	Density
Azobenzene-4,4′- dicarboxylic acid	586-91-4	Tokyo Chemical Industry (TCI)	Light yellow solid	>95%	0.02 g	1.35 g·cm^{-3}

(1) Calculating E_{α_i} and $\ln A_{\alpha_i} f_{\text{real}}(\alpha_i)$ based on Friedman method

Friedman method, a differential iso-conversion method, is applied. During the process, E_{α_i} and $\ln A_{\alpha_i} f_{\text{real}}(\alpha_i)$ are got through the linearization of $\ln(\beta \mathrm{d}\alpha_i/\mathrm{d}T_i)$ against $1/T_i$, as shown in Eq. (1):

$$\ln\left(\frac{\beta \mathrm{d}\alpha_i}{\mathrm{d}T_i}\right) = \ln A_{\alpha_i} f_{\text{real}}(\alpha_i) - \frac{E_{\alpha_i}}{RT_i},\ i = 1, 2 \tag{1}$$

where β is the heating rate, °C·min^{-1}; α_i is the conversion rate, $i = 1, 2$ represent the first and main peak stages, respectively; T_i is the temperature, K; A_{α_i} is the pre-exponential factor at each stage, s^{-1}; $f_{\text{real}}(\alpha_i)$ is the reaction mechanism; E_{α_i} is the activation energy at each stage, kJ·mol^{-1}; R is the ideal gas constant, 8.314 J·(mol·K)$^{-1}$.

(2) Determining compensation coefficients $\widehat{\beta}_0$ and $\widehat{\beta}_1$ based on compensation effect

By selecting $f_{\text{ideal}}(\alpha_i)$ and fixing a α_i, there are different $\mathrm{d}\alpha_i/\mathrm{d}t_i$ corresponding to different heating rates. Based on the kinetic compensation effect, according to Eq. (2), the intercept, denoted by $\ln A_0$, and slope, denoted by $-E_0/R$, can be obtained through linearization of $\ln[(\mathrm{d}\alpha_i/\mathrm{d}t_i)/(f_{\text{ideal}}(\alpha_i))]$ against $1/T_i$. $\ln A_0$ and E_0 also conform to a linear relationship. Therefore, for each α_i, a pair of compensation coefficients in Eq. (3) can be determined through the linearization of $\ln A_0$ against E_0:

$$\ln\left[\frac{\mathrm{d}\alpha_i/\mathrm{d}t_i}{f_{\text{ideal}}(\alpha_i)}\right] = \ln A_0 - \frac{E_0}{RT_i} \tag{2}$$

$$\ln A_{\alpha_i} = \ln\left[\frac{\dfrac{\mathrm{d}\alpha_i}{\mathrm{d}t_i}}{f_j(\alpha_i)}\right] + \frac{E_{\alpha_i}}{RT_i} = \widehat{\beta}_0 + \widehat{\beta}_1 E_{\alpha_i} \tag{3}$$

$(i = 1, 2; j = \text{real}, \text{ideal})$

where $\widehat{\beta}_0$ and $\widehat{\beta}_1$ are the compensation coefficients.

(3) Verifying $f_{\text{ideal}}(\alpha_i)$ through comparison of unknown parameters based on nonlinear fitting

Based on Eq. (3), with the combination of E_{α_i} gained in section (1), $\ln A_{\alpha_i}$ can be generated. Then $f_{\text{real}}(\alpha_i)$ can be determined by $A_{\alpha_i} f_{\text{real}}(\alpha_i)/A_{\alpha_i}$. In order to obtain the unknown parameter m or n, nonlinear fitting of $f_{\text{real}}(\alpha_i)$ was conducted according to models that $f_{\text{ideal}}(\alpha_i)$ are affiliated to. Finally, the accuracy of the mechanism function can be verified by comparing the value of m or n with that in the ideal model.

(4) Determining the formula of kinetic model

Based on aforementioned E_{α_i}, A_{α_i}, and $f_{\text{ideal}}(\alpha_i)$, according to Eq. (4), the formula expression of the kinetic model can be obtained:

$$\frac{\mathrm{d}\alpha_i}{\mathrm{d}t_i} = A_{\alpha_i} \mathrm{e}^{-\frac{E_{\alpha_i}}{RT_i}} f_{\text{ideal}}(\alpha_i) \tag{4}$$

3. Results and Discussion

3.1. The decomposition behavior and characteristic parameters of azobenzene-4,4′-dicarboxylic acid

Fig. 2 shows the curves of heat flow of ADCA with temperature at heating rates of 1.0, 2.0, 4.0, and 8.0 °C·min^{-1}.

As shown in Fig. 2, there are two consecutive, conspicuous and overlapping exothermic peaks during the thermal decomposition process of ADCA at the four heating rates. The main exothermic peak P2 shows up after the first exothermic peak P1, followed by an endothermic peak P3. Meanwhile, with the increase of heating rate, the heat flow curve becomes sharper and the exothermic peak moves toward a high-temperature direction. This may be ascribed to the increase of the temperature gradient between surface and interior of the sample at a higher heating rate. The onset temperature and end temperature of decomposition are delayed, that is, the phenomenon of "thermal lag" appears [16]. It can be seen from the exothermic peak that there is a superposition similar to the process of multi-step decomposition of ammonium perchlorate literatured in Ref. [22]. As a result, the decomposition of ADCA perhaps belongs to a multi-step process.

Table 2 lists the characteristic parameters of the decomposition of ADCA, including onset temperature, exothermic peak temperature, endothermic peak temperature, maximum heat flow, average heat flow, and half peak width.

As seen from Fig. 2 and Table 2, with the increase of heating rate, the onset temperature increases from 349.41 °C to 393.58 °C, and the main peak temperature increases from 405.00 °C to 447.86 °C. Additionally, max and average heat flow also witness a rise. The half peak width tends to be larger at relatively high heating rate.

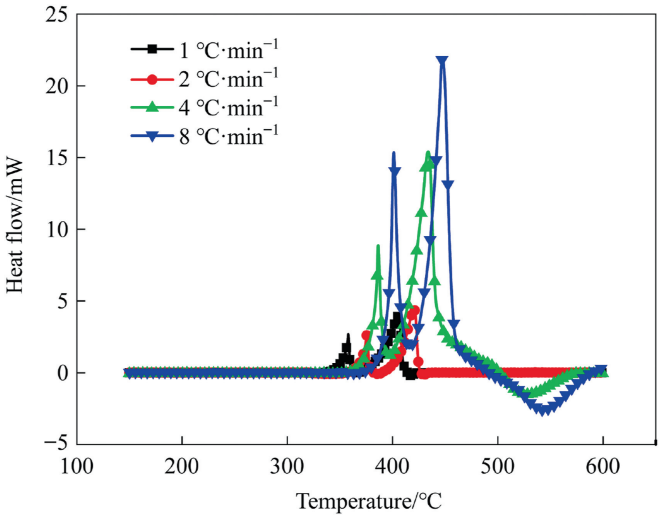

Fig. 2. Heat flow of ADCA with temperature at different heating rates.

Table 2
Characteristic parameters of ADCA thermal decomposition

Heating rate β/°C·min^{-1}	First peak					Main peak					Endothermic peak
	T_{onset1}/°C	T_{p1}/°C	H_{max1}/mW	$H_{avarage1}$/mW	$\Delta T_{1/2}$/°C	T_{onset2}/°C	T_{p2}/°C	H_{max2}/mW	$H_{avarage2}$/mW	$\Delta T'_{1/2}$/°C	T_{p3}/°C
1	349.41	358.15	2.16	0.03	5.67	385.86	405.00	3.89	0.14	13.89	417.05
2	367.25	375.69	2.25	0.04	6.70	404.12	420.28	4.49	0.13	12.97	429.71
4	378.09	386.97	6.69	0.10	7.25	414.10	433.36	13.04	0.53	16.41	528.68
8	393.58	401.02	12.67	0.24	9.20	428.93	447.86	20.54	0.83	16.44	542.50

Note: The onset temperature refers to the temperature corresponding to the intersection point between the extrapolated baseline and the tangent line of the heat flow rate curve with the maximum slope before reaching the peak.

Traditionally, D_P is used to represent the comprehensive decomposition characteristics of reactants as mentioned in a previous study [23]:

$$D_P = \frac{H_{maxi} \times H_{averagei}}{T_{onseti} \times T_{pi} \times \Delta T_{1/2}\left(\text{or } \Delta T'_{1/2}\right)},\ i = 1,2 \tag{5}$$

where, D_P is comprehensive decomposition characteristic parameter; T_{onseti} (i = 1,2) is onset temperature; T_{pi} (i = 1,2) is exothermic peak temperature; T_{p3} is endothermic peak temperature; H_{maxi} (i = 1,2) is maximum heat flow; $H_{avaragei}$ (i = 1,2) is average heat flow; $\Delta T_{1/2}$ and $\Delta T'_{1/2}$ are half peak widths.

This indicator can be used to characterize the thermal stability of substances by taking into account typical features of the heat flow curve. The larger H_{maxi} and $H_{averagei}$, the more heat is released during thermal decomposition and the stronger this process is. The smaller the T_{onset}, the easier it is for thermal decomposition to be triggered off. The smaller T_p and the larger half peak width, the earlier and more frequently the high value of heat release appears. As D_P gets larger, the thermal stability of the material gets worse.

Applying the parameters in Table 2 to the aforementioned equation, the comprehensive decomposition characteristic parameters of ADCA in two decomposition stages at four heating rates can be calculated. The results are listed in Table 3. With the increase of heating rate, the D_P of first stage increases from 9.13×10^{-8} to 2.09×10^{-6} mW$^{2\cdot}$°C^{-3}, whereas the D_P of second stage rises from 2.51×10^{-7} to 5.40×10^{-6} mW$^{2\cdot}$°C^{-3}, indicating that the thermal stability of ADCA is getting worse and worse.

3.2. Thermodynamic and kinetic parameters of azobenzene-4,4′-dicarboxylic acid. decomposition

In order to accurately obtain the thermodynamic and kinetic parameters of ADCA decomposition, overlapped exothermic peaks need to be separated. For this work mainly focuses on the exothermic peaks, thus the endothermic peaks are removed before further processing. Then the separation of the two steps of the decomposition process is achieved through mathematical fitting. The nonlinear least squares method based on Levernberg Marquardt algorithm is used for fitting and the correction determination coefficients R^2 of the Asym2Sig model are all higher than 0.98. The curves of heat flow with time after separating peaks at four heating rates are shown in Fig. 3.

The separated curves in Fig. 3 are integrated in full range to obtain the reaction heat release per unit mass, as listed in Table 4. The unit mass reaction heat release of the whole thermal decomposition process of ADCA is 182.46–231.16 J·g^{-1}, with an average of 204.67 J·g^{-1}.

At the same time, relying on the curves in Fig. 3, the real-time one-variable integral value can be calculated and the conversion rate α_i can be obtained by counting the proportion of this value in the total heat release, as shown in Fig. 4(a), (c). Afterward, the reaction rate $d\alpha_i/dt_i$ can be obtained, as shown in Fig. 4(b), (d).

According to Eq. (1), the activation energy E_{α_i} and $A_{\alpha_i}f_{real}(\alpha_i)$ of the first and main peaks at any conversion rate α_i during the thermal decomposition of ADCA are obtained, as shown in Figs. 5 and 6.

Figs. 5 and 6 indicate that the accuracy of calculation results of activation energy E_{α_i} and $A_{\alpha_i}f_{real}(\alpha_i)$ are high when the conversion rate α_1 of the first peak is no more than 0.80 or that α_2 of the main peak is no more than 0.85. The correlation coefficient R^2 of both cases is above 0.90. In the above range, with the increase of conversion rate α_1, the activation energy of the first peak decreases monotonously from 181.96 kJ·mol^{-1} to 98.87 kJ·mol^{-1}, whereas the activation energy of the main peak increases slightly from 172.61 kJ·mol^{-1} to 187.13 kJ·mol^{-1} when $\alpha_2 \leq 0.50$ and then also drops monotonously to 154.79 kJ·mol^{-1}. Polynomial fitting is executed for the curve of E_{α_i} to figure out its relationship with α_i, E_{α_i}, $A_{\alpha_i}f_{real}(\alpha_i)$, and R^2, and the relations between E_{α_i} and α_i are listed in Table 5.

3.3. Thermal kinetic model of azobenzene-4,4′-dicarboxylic acid decomposition

Considering that the actual thermal decomposition of ADCA involves a transition process from a solid phase to a gas phase, which belongs to heterogeneous reaction, analysis should be based on the kinetic-model functions for solid-state reactions. In truth, crystals usually have imperfect areas, and the reactivity of these defect areas is stronger than that of other areas, often impelling the reaction to firstly start in some defect centers, especially dislocation centers. Further reactions will be mainly confined to the reactant/product interface inside [24]. According to different ways of controlling reaction rate, the relationship between α and t can be deduced from gas diffusion, phase interface reaction, nucleation and growth, *etc.*, generating different forms of thermal kinetic-model functions of solid-phase decomposition. Koga and Tanaka [25] listed the kinetic models commonly used in solid-state reactions. Maitra *et al.* [26] also classified common kinetic models for solid-state reaction and found that the thermal decomposition process of limestone and magnesite samples followed Avrami–Erofeev model. Li *et al.* [10] concluded that the thermal decomposition process of AIBN followed the laws of autocatalysis and N-order rate law. Sanchirico [27] found that the generalized autocatalytic model was most probable for describing the thermal decomposition process of 3,5-dinitro-4-methylbenzoic acid. Through cross comparison of several papers [26,28,29], this study screened out the common kinetic-model functions that may be

Table 3
Comprehensive decomposition characteristic parameters of ADCA at different stages

Heating rate/°C·min^{-1}	D_P/mW^2·°C^{-3}	
	First peak	Main peak
1	9.13×10^{-8}	2.51×10^{-7}
2	9.74×10^{-8}	2.65×10^{-7}
4	6.31×10^{-7}	2.35×10^{-6}
8	2.09×10^{-6}	5.40×10^{-6}

used to describe the thermal decomposition of ADCA, as listed in Table 6.

According to the method in Section 2.2, each kinetic-model function in Table 6 is selected one by one and substituted into Eq. (2) and Eq. (3) for calculating the compensation parameters $\widehat{\beta}_0$ and $\widehat{\beta}_1$. The corresponding results of the first and main peaks are shown in Table 7. Further nonlinear fitting results are shown in Table 8.

According to Table 7, with the application of Avrami–Erofeev model, Mampel power law model, phase-boundary reaction model, or Sestak–Berggren (S–B) model, the kinetic parameters of ADCA show a significant compensation effect, and the linear correlation is greater than 0.9. However, it is further found through nonlinear fitting (see Table 8 for the results) that the unknown parameters obtained are different from the parameters of the ideal model. The deviation of the phase-boundary reaction model is too large, and thus it is ruled out. In the remaining models, the fitting degrees of nonlinear fitting for the first peak above 0.97 correspond to A3, A4, P3, and P4 models. For the main peak, the filtering results are A3, A4, P2 and S–B models.

The Mampel power law model, namely the power function mechanism function, is a very simple model, which is developed from the multi-step nucleation theory. Galwey and Brown [30] believed that the germ nucleus could host p product atoms (ions or molecules) and then was converted into a growth nucleus when the number reached p. The rate coefficients of single-atom addition were equal as the scholar assumed. The nucleation rate is expressed as $dN/dt = C\eta t^{\eta-1}$, where C is constant, η is the step number involved in the process of nucleation, usually taken as 2 or 3. Combined with the interface advance rate equation, the power law is more generally expressed as $\alpha^{1/n} = kt$, in which $n = \eta + \lambda$ (η and λ denote the law of nucleation and the dimension of nuclear growth, respectively). In consideration of the induction period, heating time and so on, t_0 is introduced, and then the rate equation is transformed to $\alpha = k^n(t - t_0)^n$ [30]. However, the assumption that the growth nucleus is formed instantly, and the advancing speed of the interface in three-dimensional space is unrestricted, differs a lot from the actual situation. Compared with Mampel power law model, the Avrami–Erofeev model is more consistent with the description of actual process of ADCA thermal decomposition, where it takes a certain time to decompose. Besides, in practice, nucleation is not a transient process, and the growth of the

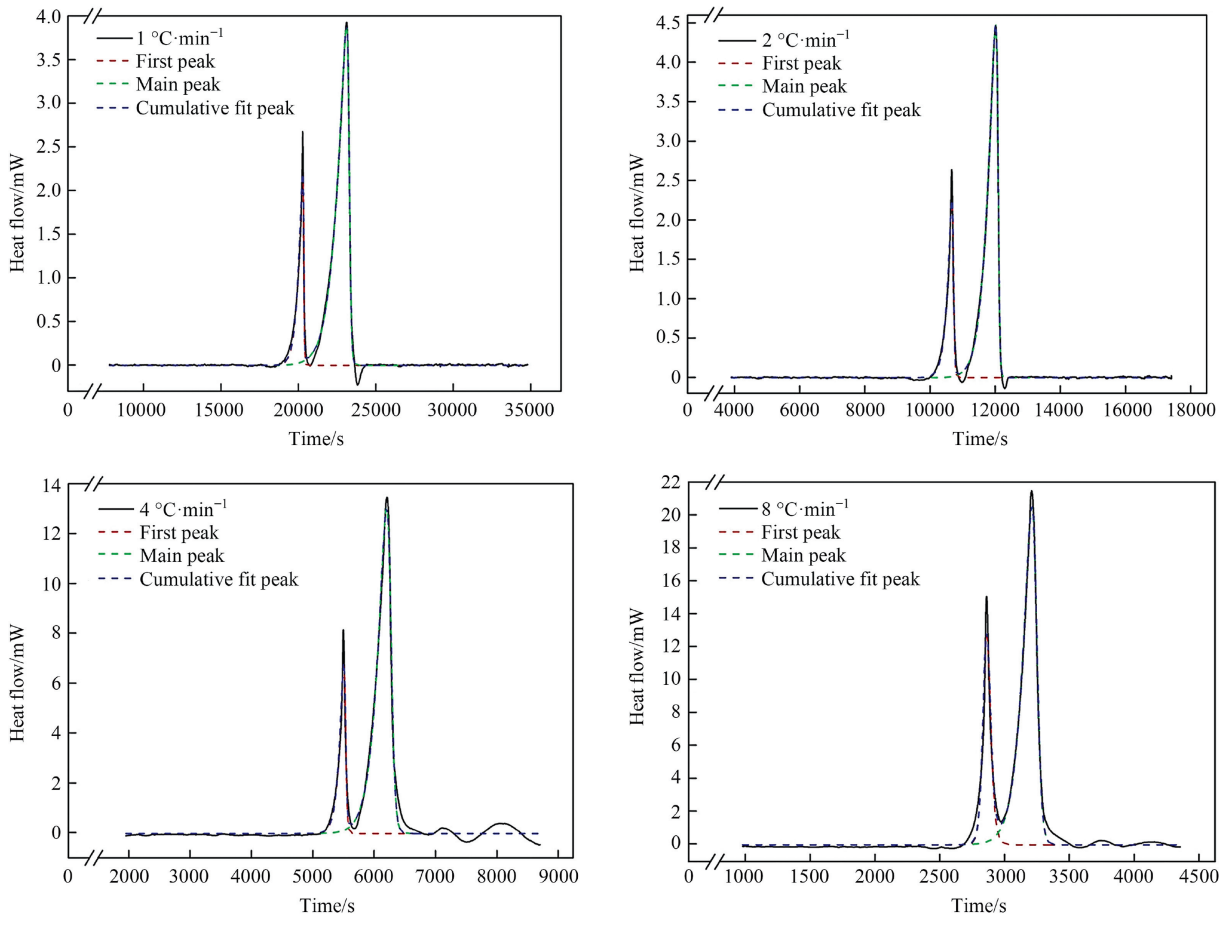

Fig. 3. The curves of heat flow with time for ADCA decomposition at four heating rates.

Table 4
Unit mass heat release of ADCA thermal decomposition at four heating rates

Heating rate/°C·min^{-1}	Total unit mass heat release ΔH/J·g^{-1}
1	220.80
2	184.25
4	231.16
8	182.46

nucleus is limited. As to the Avrami–Erofeev model, the fitting degree of nonlinear fitting for A4 is higher than that for A3, indicating that it can more accurately describe the thermal decomposition process of ADCA.

At the same time, the fitting degree of the S–B model is relatively high as well. However, this model is only a mathematical generalization of other models [31], and when it takes $f(\alpha) = 4\alpha^{0.01}(1-\alpha)[-\ln(1-\alpha)]^{0.75}$, eventually, the fitting degrees of nonlinear fitting for the first and main peaks are above 0.99. Therefore, it reaches an agreement with A4 model to some extent, in other words, A4 model is more appropriate for the first and main peaks.

The A4 model is introduced in Eqs. (2) and (3) to obtain the compensation parameters, and then the pre-exponential factors A_{α_1}, A_{α_2} are obtained according to E_{α_i} and compensation parameters. Based on A_{α_1}, A_{α_2}, $f_{\text{ideal}}(\alpha_i)$, E_{α_i}, *etc.*, the multi-step reaction-rate model of ADCA decomposition can be established [32], as shown in Eqs. (6)–(8):

$$\begin{aligned} A_{\alpha_1} &= \exp(-5.16054 + 0.18057 \times E_1) \\ &= \exp\left(27.920 - 7.691\alpha_1 + 16.995\alpha_1^2 - 40.377\alpha_1^3\right) \end{aligned} \tag{6}$$

$$\begin{aligned} A_{\alpha_2} &= \exp(-5.13435 + 0.16567 \times E_2) \\ &= \exp\left(24.094 + 0.968\alpha_2 + 26.436\alpha_2^2 - 41.542\alpha_2^3\right) \end{aligned} \tag{7}$$

$$\begin{aligned} \frac{d\alpha}{dt} &= \gamma\frac{d\alpha_1}{dt_1} + (1-\gamma)\frac{d\alpha_2}{dt_2} \\ &= \gamma A_{\alpha_1} e^{-\frac{E_{\alpha_1}}{RT_1}} f(\alpha_1) + (1-\gamma)A_{\alpha_2} e^{-\frac{E_{\alpha_2}}{RT_2}} f(\alpha_2) \\ &= 0.856\exp 27.920 - 7.691\alpha_1 + 16.995\alpha_1^2 - 40.377\alpha_1^3 \times \\ &\quad \exp\left(-\frac{22034.640}{T} + \frac{5123.166}{T}\alpha_1 - \frac{11320.423}{T}\alpha_1^2 + \frac{26895.478}{T}\alpha_1^3\right) \times \\ &\quad (1-\alpha_1)[-\ln(1-\alpha_1)]^{\frac{3}{4}} + \\ &\quad 3.144\exp\left(24.094 + 0.968\alpha_2 + 26.436\alpha_2^2 - 41.542\alpha_2^3\right) \times \\ &\quad \exp\left(-\frac{21220.111}{T} - \frac{702.550}{T}\alpha_2 - \frac{19193.288}{T}\alpha_2^2 + \right. \\ &\quad \left.\frac{30160.452}{T}\right)\alpha_2^3(1-\alpha_2)[-\ln(1-\alpha_2)]^{\frac{3}{4}} \end{aligned} \tag{8}$$

where γ is contribution degree, $\gamma = Q_1/(Q_1+Q_2)$,Q_1 and Q_2 are the thermal effects of two stages respectively, J·g^{-1}.

3.4. Reaction mechanism of azobenzene-4,4′-dicarboxylic acid thermal decomposition

As shown in Fig. 1, azos such as ADCA are typically characterized by N=N bond. Analyzing the micro-process of thermal decomposition of ADCA, in fact, with the increase of temperature, the amplitude of atoms vibration in ADCA will intensify. According to the bond energy and bond-breaking process of azos literatured in the past, the C–C bond outside the benzene ring may be broken first, followed by the breakage of C–N or N=N bond [16,17,33]. In detail, the C–C bond outside the benzene ring may break and produce COOH· and ·ph–N=N–ph·.

In addition, bond fracture and the intensification of molecular thermal motion can trigger lattice deformation and greater fluctuation of force field, resulting in defects such as point defects, dislocations, etc. As mentioned earlier, the reactivity is higher in defect or imperfect areas. In these regions, the aggregates formed by COOH and ph–N=N–ph remain embedded in the original reactant's matrix, usually with sufficient mobility, and have the potential to reorganize into the nucleus of the product phase. This process can follow the linear or exponential nucleation law.

As more products are added to the reactant/product interface to facilitate the growth of existing nuclei, the interface expands outward along the three-dimensional direction at an equal (constant) rate. This process is similar to the explanation of A4 model [30].

Meanwhile, the growth of nuclei and the advance of the interface may cause stress in the crystal. Under the combined effects of sufficiently large stress and temperature, the relatively fragile bond chains are further broken and may form substances with smaller molecular weight, accompanied by the formation of gaseous products [34]. For example, C–N bond fracture generates ph—ph and N_2, or N=N bond fracture generates ·ph–N:, ·ph–NH·, leading to the formation of COOH–ph–NH_2 and CO_2.

The aforementioned process steadily goes on by obeying the multi-step overall reaction rate model of ADCA decomposition established earlier, further inducing that the defects extend to the surface and that cracks form at the fracture points. The gas emission will also trigger the rearrangement of lattice cell structures from reactants to products. The unit-cell transforms from a larger shape into a smaller one, and the volume contracts [35]. At the same time, the pre-melting phenomenon on grain boundary may occur around dislocation. There is no endothermic peak near the melting point due to the simultaneous occurrence of exothermic and endothermic processes [36]. In conclusion, it is inferred that the micro-process of ADCA decomposition is as follows (Fig. 7).

4. Thermal Safety Assessment of Azobenzene-4,4′-dicarboxylic acid

During the whole life-cycle of production, storage, transportation, and use of ADCA, thermal accumulation may lead to thermal spontaneous combustion or thermal explosion. To evaluate its thermal hazard, SADT is usually adopted. In F-K thermal spontaneous combustion theory, it is assumed that there is a temperature gradient in the system and that the temperature at boundary is equal to ambient temperature. According to the assumption, the F-K model is more available for describing the thermal spontaneous combustion process of solid reactants [37]. In this work, the F-K model is used to analyze the thermal hazard of ADCA.

Due to the complexity of solving the heat balance equation by using corresponding boundary conditions, the F-K dimensionless parameter δ is used to calculate the SADT of ADCA. The calculation formula is as follows [38]:

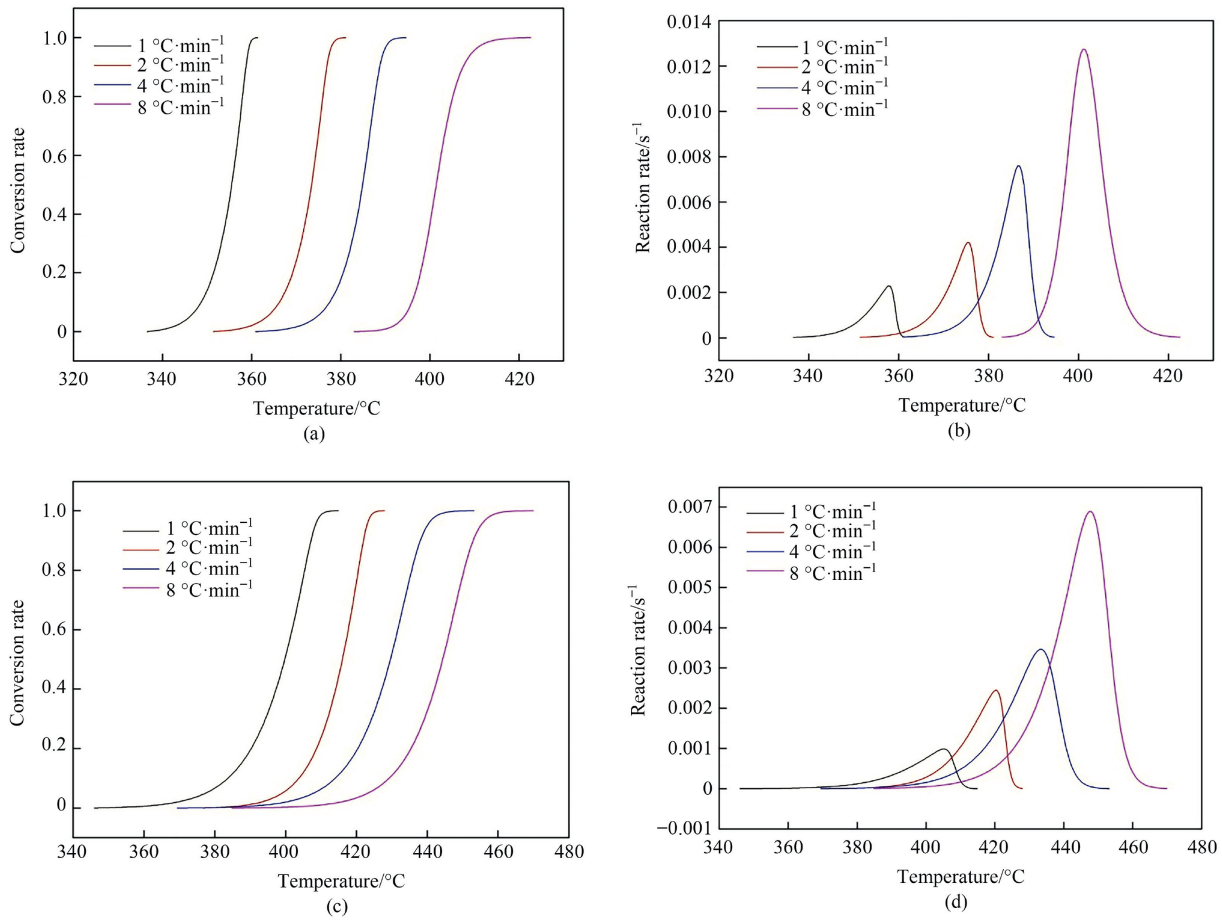

Fig. 4. Conversion rate and reaction rate with temperature of ADCA thermal decomposition at four heating rates ((a) first peak conversion rate diagram, (b) first peak reaction rate diagram, (c) main peak conversion rate diagram, (d) main peak reaction rate diagram).

$$\delta = \frac{a_0^2 \Delta H E \rho A \exp(-E/RT_0)}{\lambda R T_0^2} \tag{9}$$

where a_0 is the radius for cylinder, m; ρ is density, g·cm^{-3}; T_0 is ambient temperature of the system, namely SADT, °C; λ is thermal conductivity of reactants, W·m^{-1}·K^{-1}.

In this work, taking the actual situation into account, the formula corresponding to the finite cylinder ($l < d$) ($\delta_c = 0.88 + 1.90(l/d)^2$) is selected [39]. If the value of actual parameter is greater than that of critical parameter, the system will catch fire.

Substituting every parameter into the solution, the critical parameter can be approached closely through temperature iteration, and SADT can be determined simultaneously. The thermal

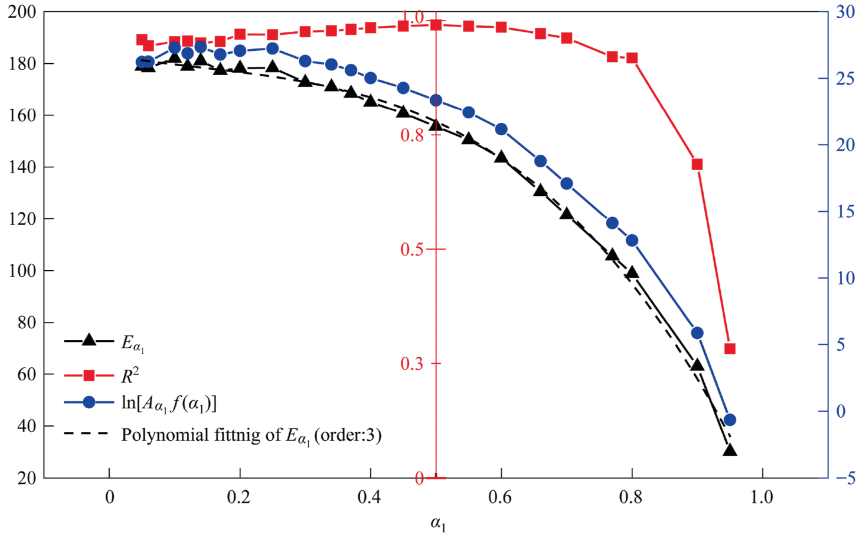

Fig. 5. The activation energy E_{α_i} and $A_{\alpha_i} f_{\text{real}}(\alpha_i)$ change of the first peak for ADCA thermal decomposition.

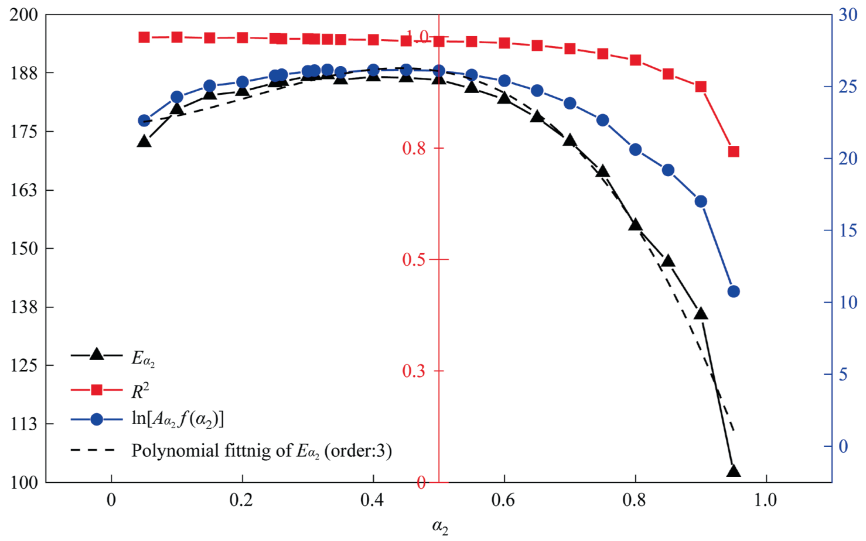

Fig. 6. The activation energy E_{α_i} and $A_{\alpha_i} f_{\text{real}}(\alpha_i)$ change of the main peak for ADCA thermal decomposition.

conductivity of reactant is taken as 0.3 $W \cdot m^{-1} \cdot K^{-1}$. When selling ADCA in large quantities, a 25-kg cylindrical barrel, with a diameter of 38 cm and a height of 45 cm, is usually used as the transport package by market manufacturers. After calculation, the filling height is about 16.34 cm, so the critical parameter is 1.23. The average values of activation energy $\overline{E_{\alpha_i}}$ and $\overline{E}$ at the initial stage (α_i is between 0.05 and 0.25) are applied. $\overline{E}$ is about 360.50 $J \cdot g^{-1}$. According to Ref. [40], the pre-exponential factor A can be calculated through Eq. (10), with the result of 7.39×10^{24} s^{-1}:

$$A = \frac{\overline{A_{\alpha_1}} \exp\left(-\frac{\overline{E_{\alpha_1}}}{R \min(T_{\text{onset}i})}\right) + \overline{A_{\alpha_2}} \exp\left(-\frac{\overline{E_{\alpha_2}}}{R \min(T_{\text{onset}i})}\right)}{\exp\left(-\frac{\overline{E}}{R \min(T_{\text{onset}i})}\right)} \tag{10}$$

Table 5
Thermodynamic and kinetic parameters of ADCA decomposition

Stage	E_{α_i}/kJ·mol^{-1}	$A_{\alpha_i} f_{\text{real}}(\alpha_i)$	R^2	E_{α_i} *vs.* α_i
First peak ($\alpha_1 \leq 0.8$)	98.87–181.96	3.64×10^5–7.53×10^{11}	≥0.92	$E_{\alpha_1} = 183.20 - 42.59\alpha_1 + 94.12\alpha_1^2 - 223.61\alpha_1^3$
Main peak ($\alpha_2 \leq 0.85$)	154.79–187.13	2.15×10^8–2.29×10^{11}	≥0.92	$E_{\alpha_2} = 176.42 + 5.84\alpha_2 + 159.57\alpha_2^2 - 250.75\alpha_2^3$

Table 6
Common kinetic-model functions for describing ADCA thermal decomposition

No.	Code name	Model name	$f_{\text{ideal}}(\alpha)$	Parameter
1	A2	Avrami–Erofeev	$m \times (1-\alpha) \times [-\ln(1-\alpha)]^n$	$m = 2, n = 1/2$
2	A3			$m = 3, n = 2/3$
3	A4			$m = 4, n = 3/4$
4	P2	Mampel power law	$\frac{1}{n} \times \alpha^{1-n}$	$n = 1/2$
5	P3			$n = 1/3$
6	P4			$n = 1/4$
7	R2	Phase-boundary reaction, cylindrical symmetry	$n_2 \times (1-\alpha)^{1-n_1}$	$n_1 = 1/2, n_2 = 2$
8	R3	Phase-boundary reaction, spherical symmetry		$n_1 = 1/3, n_2 = 3$
9	D1	Parabolic rule, one-dimensional diffusion	$\frac{1}{2} \times \alpha^{-1}$	–
10	D2	Valensi equation, two-dimensional diffusion	$[-\ln(1-\alpha)]^{-1}$	–
11	D3	Jander three-dimensional diffusion	$\frac{3}{n} \times (1-\alpha)^{\frac{2}{3}} \times \left[1-(1-\alpha)^{\frac{1}{3}}\right]^{1-n}$	$n = 2$
12	F1	Order-of-reaction model	$(1-\alpha)^n$	$n = 1$
13	F2			$n = 2$
14	S-B	Sestak–Berggren	$\alpha^m \times (1-\alpha)^n$	$m = 1, n = 1$
15	G-A-1	Generalized autocatalytic model	$(1-\alpha)^{n_1} \times (\alpha^{n_2} + z)$	$n_1 = 1, n_2 = 1, z = 0.5$
16	G-A-2			$n_1 = 2, n_2 = 2, z = 0.5$

Table 7
Compensation parameters for different models of ADCA thermal decomposition

No.	Code number	First peak			Main peak		
		$\widehat{\beta}_0$	$\widehat{\beta}_1$	Linear correlation Adj. R^2	$\widehat{\beta}_0$	$\widehat{\beta}_1$	Linear correlation Adj. R^2
1	A2	−3.39012	0.17223	0.99871	−2.93164	0.15619	0.98758
2	A3	−4.51377	0.17779	0.99981	−4.34344	0.16251	0.99905
3	A4	−5.16054	0.18057	0.99999	−5.13435	0.16567	0.99986
4	P2	−6.07729	0.18641	0.9995	−8.69784	0.18552	0.99922
5	P3	−6.94865	0.19066	0.99998	−9.60473	0.1893	0.99349
6	P4	−7.46928	0.19278	0.99996	−10.14312	0.1912	0.98861
7	R2	−2.9576	0.16461	0.99068	−3.55305	0.15571	0.93494
8	R3	−2.78906	0.16159	0.98976	−2.745	0.14956	0.91399
9	D1	−0.49797	0.1482	0.94584	−2.79879	0.1515	0.73727
10	D2	0.32261	0.14032	0.935	−0.46218	0.13628	0.63216
11	D3	0.56404	0.13112	0.92096	1.74373l	0.11744	0.48913
12	F1	−0.54244	0.15555	0.98767	0.78065	0.13724	0.85916
13	F2	2.90159	0.13743	0.97879	8.06175	0.1003	0.57782
14	S-B	−3.3378	0.18103	0.99962	−2.22784	0.15993	0.99741
15	G-A-1	−1.91054	0.16523	0.99425	−1.35418	0.14977	0.9467
16	G-A-2	1.65763	0.14776	0.98515	5.15407	0.11847	0.75597

Through iteration, the temperatures corresponding to critical parameters at different heating rates are obtained (as shown in Table 9). The average value is about 287.00 °C. Therefore, when the environment temperature of ADCA storage in a 25-kg cylindrical barrel reaches 287 °C, self-accelerating decomposition can be activated. Without further loss prevention, it will eventually lead to

Table 8
Nonlinear fitting accuracy of different models for ADCA

No.	Code number	First peak		Main peak	
		Unknown parameters	Fitting degree Adj. R^2	Unknown parameters	Fitting degree Adj. R^2
1	A2	$m = 2.2267$; $n = 0.55809$	0.88113	$m = 2.34084$; $n = 0.66849$	0.93989
2	A3	$m = 3.09756$; $n = 0.67683$	0.97941	$m = 3.13757$; $n = 0.71633$	0.98981
3	A4	$m = 4.02474$; $n = 0.75037$	0.99855	$m = 3.96854$; $n = 0.74495$	0.99643
4	P2	$n = 0.48557$	0.95296	$n = 0.52193$	0.97893
5	P3	$n = 0.33259$	0.99761	$n = 0.3711$	0.91099
6	P4	$n = 0.25109$	0.99653	$n = 0.28597$	0.87011
7	R2	$n_1 = 0.77248$; $n_2 = 1.8497$	0.05534	$n_1 = 0.98791$; $n_2 = 1.52131$	−0.05494
8	R3	$n_1 = 0.69089$; $n_2 = 2.67595$	0.12021	$n_1 = 0.928$; $n_2 = 2.14949$	−0.03692
14	S–B	$m = 1.02963$; $n = 1.01135$	0.95516	$m = 0.99334$; $n = 1.0448$	0.97598

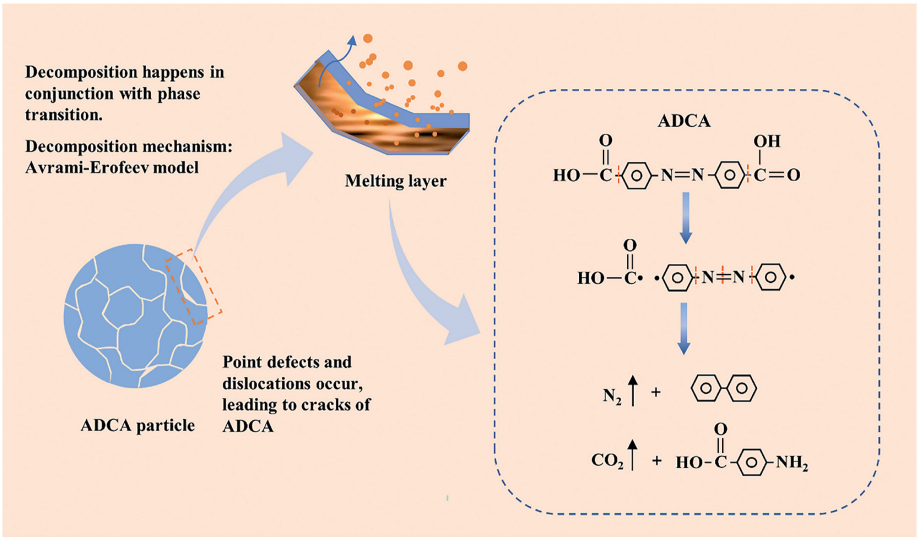

Fig. 7. Inference on thermal decomposition process of ADCA.

Table 9
Temperatures corresponding to critical parameters at different heating rates

Heating rate/°C·min^{-1}	Temperatures corresponding to critical parameter/°C
1	286.40
2	287.70
4	286.00
8	287.80

thermal spontaneous combustion or thermal explosion accidents of ADCA.

5. Conclusions

In the work, the thermal decomposition behavior of ADCA was studied by using the SENSYS evo DSC instrument. The thermal characteristic parameters of decomposition process were extracted, and thermodynamic and kinetic analyses were carried out accordingly. Besides, the overall reaction rate equation was obtained, and the thermal decomposition mechanism was inferred. Furthermore, based on F-K theory, the SADT of ADCA was calculated to characterize its thermal hazard. The main conclusions are as follows:

(1) There are two overlapping exothermic peaks and one endothermic peak in the thermal decomposition process of ADCA, indicating its multi-step decomposition process. The comprehensive decomposition characteristic parameter D_P increases with the increase of heating rate, representing the thermal stability of ADCA becoming worse.
(2) The activation energies of the first and main peaks decrease with the increase of α. The overall heat release per unit mass is 182.46–231.16 J·g^{-1}.
(3) The thermal decomposition process of the first and the main peaks follows Avrami–Erofeev model, and the overall reaction rate expression can be written as follows:

$$\frac{d\alpha}{dt} = 0.856\exp\left(27.920 - 7.691\alpha_1 + 16.995\alpha_1^2 - 40.377\alpha_1^3\right)\times \exp\left(-\frac{22034.640}{T} + \frac{5123.166}{T}\alpha_1 - \frac{11320.423}{T}\alpha_1^2 + \frac{26895.478}{T}\alpha_1^3\right)\times (1-\alpha_1)[-\ln(1-\alpha_1)]^{\frac{3}{4}} + 3.144\exp\left(24.094 + 0.968\alpha_2 + 26.436\alpha_2^2 - 41.542\alpha_2^3\right)\times \exp\left(-\frac{21220.111}{T} - \frac{702.550}{T}\alpha_2 - \frac{19193.288}{T}\alpha_2^2 + \frac{30160.452}{T}\alpha_2^3\right)\times (1-\alpha_2)[-\ln(1-\alpha_2)]^{\frac{3}{4}}$$

(4) Based on the F–K model, the SADT of ADCA is about 287.0 °C when packed in 25-kg barrels.

Declaration of Interest

The authors declare that they have no known competing financial interests or personal relationships that could have appeared to influence the work reported in this paper.

Acknowledgements

This work was supported by National Natural Science Foundation of China (51974166).

Nomenclature

A_{α_i}	pre-exponential factor at each stage, s^{-1}
a_0	radius for cylinder, m
D_P	comprehensive decomposition characteristic parameter, mW^2·°C^{-3}
E_{α_i}	activation energy at each stage, kJ·mol^{-1}
$f_{real}(\alpha_i)$, $f_{ideal}(\alpha_i)$	reaction mechanism
$H_{averagei}$, $H_{max\ i}$	average heat flow and maximum heat flow, mW
ΔH	unit mass heat release, J·g^{-1}
R	ideal gas constant, 8.314 J·mol^{-1}·K^{-1}
T_i	temperature at each stage °C, i = 1,2
T_{onseti}	onset temperature, °C
T_{pi}	peak temperature, °C
T_0	ambient temperature of the system, °C
$\Delta T_{1/2}$, $\Delta T'_{1/2}$	half peak width of the first and main peak, °C
α_i	conversion rate
β	heating rate, °C·min^{-1}
$\widehat{\beta}_0$, $\widehat{\beta}_1$	compensation coefficients
γ	contribution degree
δ	F–K dimensionless parameter
λ	thermal conductivity of reactants, W·m^{-1}·K^{-1}
ρ	density, g·cm^{-3}
δ	F–K dimensionless parameter

References

[1] S.H. Liu, C.R. Cao, W.C. Lin, C.M. Shu, Experimental and numerical simulation study of the thermal hazards of four azo compounds, *J. Hazard. Mater.* 365 (2019) 164–177.
[2] A. Khayyami, M. Karppinen, Reversible photoswitching function in atomic/molecular-layer-deposited ZnO: Azobenzene superlattice thin films, *Chem. Mater.* 30 (17) (2018) 5904–5911.
[3] H.B. Cheng, S.C. Zhang, J. Qi, X.J. Liang, J. Yoon, Advances in application of azobenzene as a trigger in biomedicine: Molecular design and spontaneous assembly, *Adv. Mater.* 33 (26) (2021) e2007290.
[4] F. Parsa, M. Ghorbanloo, M.Y. Masoomi, A. Morsali, P.C. Junk, J. Wang, Ultrasound-assisted synthesis and characterization of a new metal-organic framework based on azobenzene-4, 4-dicarboxylic acid: Precursor for the fabrication of Co_3O_4 nano-particles, *Ultrason. Sonochem.* 45 (2018) 197–203.
[5] R. Mogale, J. Conradie, E.H.G. Langner, *Trans-cis* kinetic study of azobenzene-4, 4′-dicarboxylic acid and aluminium and zirconium based azobenzene-4, 4′-dicarboxylate MOFs, *Molecules* 27 (4) (2022) 1370.
[6] F. Stoessel, Thermal Safety of Chemical Processes, Wiley, Germany, 2008.
[7] The Second Subsidiary of Supervision and Administration Department of the State Administration of Work Safety, Investigation Report on the "July 22" Special Major Sleeper Bus Combustion Accident in Xinyang, Henan Province, Beijing-Zhuhai Expressway, 2012. https://www.mem.gov.cn/gk/sgcc/tbzdsgdcbg/2012/201206/t20120627_245231.shtml.
[8] S.H. Liu, W.C. Lin, H.Y. Hou, C.M. Shu, Comprehensive runaway kinetic analysis and validation of three azo compounds using calorimetric approach and simulation, *J. Loss Prev. Process. Ind.* 49 (2017) 970–982.
[9] S.H. Liu, C.M. Shu, Advanced technology of thermal decomposition for AMBN and ABVN by DSC and VSP2, *J. Therm. Anal. Calorim.* 121 (1) (2015) 533–540.
[10] X.R. Li, X.L. Wang, H. Koseki, Study on thermal decomposition characteristics of AIBN, *J. Hazard. Mater.* 159 (1) (2008) 13–18.
[11] A.D. Yu, W.J. Wang, M. Hua, X.H. Pan, X.M. Liang, C.Y. Wei, C.M. Shu, J.C. Jiang, Thermal hazard analysis of 1-((cyano-1-methylethyl) azo) formamide and effect of incompatible substances on its thermal decomposition, *J. Loss Prev. Process. Ind.* 65 (2020) 104098.
[12] D. Çanakçı, Synthesis, spectroscopic, thermodynamics and kinetics analysis study of novel polymers containing various azo chromophore, *Sci. Rep.* 10 (2020) 477.
[13] B. Roduit, M. Hartmann, P. Folly, A. Sarbach, P. Brodard, R. Baltensperger, Thermal decomposition of AIBN, part B: Simulation of SADT value based on DSC results and large scale tests according to conventional and new kinetic merging approach, *Thermochim. Acta* 621 (2015) 6–24.

[14] H.B. Li, W.Q. Wu, X. Peng, X. Wang, X.Y. Guo, L.P. Chen, W.H. Chen, Research on the decomposition kinetics and thermal hazards of 2, 2′-azobis(2-methylpropionamidine) dihydrochloride by experimental and simulation approach, *Thermochim. Acta* 689 (2020) 178595.
[15] N.C. Zhou, M. Hua, A.D. Yu, W.J. Wang, X.H. Pan, C.Y. Wei, J.C. Jiang, Effects of incompatible substances on thermal stability of dimethyl 2, 2′-azobis(2-methylpropionate) (AIBME) in the application process, *J. Loss Prev. Process. Ind.* 71 (2021) 104478.
[16] H.M. Sun, S. Guo, S.N. Chen, M. Jia, S.Y. Shen, Thermal behavior and decomposition mechanism of azobenzene by using kinetic calculation method and molecular dynamics simulation method, *Process. Saf. Environ. Prot.* 161 (2022) 447–453.
[17] M. Jia, S. Guo, S. Gao, Q.S. Wang, J.H. Sun, Thermal decomposition mechanism of diisopropyl azodicarboxylate and its thermal hazard assessment, *Thermochim. Acta* 688 (2020) 178601.
[18] Y. Tian, D.F. Zhao, C.M. Shu, N. Roy, M. Qi, Y. Liu, Study on thermal stability and thermal decomposition mechanism of 1-((cyano-1-methylethyl) azo) formamide, *Process. Saf. Environ. Prot.* 155 (2021) 219–229.
[19] Y. Do Kim, J.J. Lee, An investigation on thermal decomposition behavior of water-soluble azo dyes, *Fibres. Polym.* 24 (8) (2023) 2799–2806.
[20] J. Ding, X.C. Zhang, D.F. Hu, S.L. Ye, J.C. Jiang, Model-free kinetic determination of pre-exponential factor and reaction mechanism in accelerating rate calorimetry, *Thermochim. Acta* 702 (2021) 178983.
[21] N. Sbirrazzuoli, Determination of pre-exponential factors and of the mathematical functions $f(\alpha)$ or $G(\alpha)$ that describe the reaction mechanism in a model-free way, *Thermochim. Acta* 564 (2013) 59–69.
[22] H.B. Li, X.Q. Zhao, W.Q. Wu, S.R. Li, L.P. Chen, W.H. Chen, Experimental research on multistep decomposition kinetics of ammonium perchlorate in the space-confined environment, *J. Therm. Anal. Calorim.* 147 (20) (2022) 11535–11547.
[23] X.W. Yao, K.L. Xu, F. Yan, Z.Q. He, Pyrolysis characteristics and kinetics comparison of different agricultural biomass wastes, *J. Northeast. Univ.* 37 (11) (2016) 1593–1597.
[24] W. Ng, Thermal decomposition in the solid state, *Aust. J. Chem.* 28 (6) (1975) 1169.
[25] N. Koga, H. Tanaka, Accommodation of the actual solid-state process in the kinetic model function, *J. Therm. Anal.* 41 (2) (1994) 455–469.
[26] S. Maitra, A.J. Pal, N. Bandyopadhyay, S. Das, J. Pal, Use of genetic algorithm to determine the kinetic model of solid-state reactions, *J. Am. Ceram. Soc.* 90 (5) (2007) 1611–1614.
[27] R. Sanchirico, On the use of the generalized autocatalytic models: The thermal decomposition of 3, 5-dinitro-4-methylbenzoic acid, *AlChE. J.* 61 (4) (2015) 1300–1308.
[28] P.J. Skrdla, R.T. Robertson, Dispersive kinetic models for isothermal solid-state conversions and their application to the thermal decomposition of oxacillin, *Thermochim. Acta* 453 (1) (2007) 14–20.
[29] R.Z. Hu, Q.Z. Shi, Thermal Analysis Dynamics, Science Press, Beijing, 2008.
[30] A.K. Galwey, B.F. Brown, Thermal Decomposition of Ionic Solid, Elsevier, Amsterdam, 1999.
[31] J. Šesták, G. Berggren, Study of the kinetics of the mechanism of solid-state reactions at increasing temperatures, *Thermochim. Acta* 3 (1) (1971) 1–12.
[32] N.V. Muravyev, N. Koga, D.B. Meerov, A.N. Pivkina, Kinetic analysis of overlapping multistep thermal decomposition comprising exothermic and endothermic processes: Thermolysis of ammonium dinitramide, *Phys. Chem. Chem. Phys.* 19 (4) (2017) 3254–3264.
[33] A.M.J. Ali, Z.Y. Al-Saigh, Photodecomposition of azobenzenes, *J. Chem. Technol. Biotechnol.* 30 (1) (1980) 440–446.
[34] Z.R. Yu, Y.L. Wang, J. Zhou, L.N. Zhou, Research progress of organic crystal defects, *Chem. Ind. Eng.* 37 (2) (2020) 19–29.
[35] K.S.P. Karunadasa, C.H. Manoratne, H.M.T.G.A. Pitawala, R.M.G. Rajapakse, Thermal decomposition of calcium carbonate (calcite polymorph) as examined by *in situ* high-temperature X-ray powder diffraction, *J. Phys. Chem. Solids* 134 (2019) 21–28.
[36] Y.L. Lu, H. Mu, H.X. Hou, Z. Chen, Study of pre-melting and melting of grain boundary through crystal phase field simulation, *Acta Metall. Sin.* 49 (3) (2013) 358–364.
[37] J.H. Sun, S.X. Lu, Z.H. Sun, Thermal risk assessment method of self-reactive chemical substances, *China Saf. Sci.* 13 (4) (2003) 44–47.
[38] P.F. Huang, P. Ping, K. Li, H.D. Chen, Q.S. Wang, J. Wen, J.H. Sun, Experimental and modeling analysis of thermal runaway propagation over the large format energy storage battery module with $Li_4Ti_5O_{12}$ anode, *Appl. Energy* 183 (2016) 659–673.
[39] H.G. Fisher, D.D. Goetz, Determination of self-accelerating decomposition temperatures for self-reactive substances, *J. Loss Prev. Process. Ind.* 6 (3) (1993) 183–194.
[40] N. Sbirrazzuoli, Determination of pre-exponential factor and reaction mechanism in a model-free way, *Thermochim. Acta* 691 (2020) 178707.